fractal and fractional

MDPI

Article

Fractional Transformation-Based Intelligent H-Infinity Controller of a Direct Current Servo Motor

Muhammad Zia Ur Rahman [1,2,*], Víctor Leiva [3,*], Carlos Martin-Barreiro [4,5], Imran Mahmood [1], Muhammad Usman [1] and Mohsin Rizwan [2]

[1] Department of Mechanical, Mechatronics and Manufacturing Engineering, University of Engineering and Technology Lahore, Faisalabad 38000, Pakistan
[2] Department of Mechatronics and Control Engineering, University of Engineering and Technology Lahore, Lahore 54890, Pakistan
[3] School of Industrial Engineering, Pontificia Universidad Católica de Valparaíso, Valparaíso 2362807, Chile
[4] Faculty of Natural Sciences and Mathematics, Escuela Superior Politécnica del Litoral ESPOL, Guayaquil 090902, Ecuador
[5] Faculty of Engineering, Universidad Espíritu Santo, Samborondón 0901952, Ecuador
* Correspondence: ziaurrahman@uet.edu.pk (M.Z.U.R.); victor.leiva@pucv.cl or victorleivasanchez@gmail.com (V.L.)

Abstract: Direct current (DC) servo motors are central to many complex systems, such as electrical, electro-mechanical, and electro-hydraulic frameworks. In practice, these systems can have nonlinear characteristics and parameter variations. Accurate model representation and position tracking of DC motors are the main issues in many real systems, such as twin rotors, aircraft, airships, and robot manipulators. The precise position tracking of these systems has already been achieved using conventional H-infinity (H_∞) controllers. However, the order and structure become more intricate when employing complex weights to shape the closed-loop system, which limits the current proposals. To overcome the above-mentioned limitations, in this article, we provide a precise angular position tracking of a DC servo motor utilizing an intelligent, robust linear controller based on a fixed-structure linear fractional transformation. The conventional H_∞ controllers are based on the minimization of an unstructured linear fractional transformation objective function that leads to a complex design of these controllers. The main advantage of the proposed intelligent H_∞ synthesis is the fixed and simple structure that increases its practical implementation. The methodology is formulated in the `MATLAB` software for the robust design of the proposed synthesis based on an intelligent fixed-structure H_∞ optimization. Simulation results are compared with conventional H_∞ and proportional-integral-derivative controllers. The results are also validated experimentally.

Keywords: fixed-structured controllers; H_∞ controller; linear fractional transformation; mayfly optimization; non-smooth H_∞ optimization; proportional derivative integral controller

MSC: 13P25

Citation: Rahman, M.Z.U.; Leiva, V.; Martin-Barreiro, C.; Mahmood, I.; Usman, M.; Rizwan, M. Fractional Transformation-Based Intelligent H-Infinity Controller of a Direct Current Servo Motor. *Fractal Fract.* **2023**, *7*, 29. https://doi.org/10.3390/fractalfract7010029

Academic Editors: Clara Ionescu, Cristina I. Muresan and Isabela Roxana Birs

Received: 9 November 2022
Revised: 12 December 2022
Accepted: 20 December 2022
Published: 28 December 2022

1. Nomenclature, Introduction, and Objectives

1.1. Nomenclature

Table 1 presents the abbreviations/acronyms considered in this article to facilitate its reading.

Table 1. Definitions of abbreviations and acronyms used in the present document.

Abbreviation/Acronym	Definition
AC	Alternating current
A/D	Analog to digital
D/A	Digital to analog

Table 1. *Cont.*

Abbreviation/Acronym	Definition
DC	Direct current
EMF	Electromotive force
GA	Genetic algorithm
H_∞	Hardy space of matrix-value functions
I/O	Input to output
LFT	Linear fractional transformation
LTI	Linear time invariant
MIMO	Multi-input multi-output
MSS	Modular servo system
PCI	Peripheral component interconnect
PID	Proportional integral derivative
PSO	Particle swarm optimization
PWM	Pulse-width modulation
$R(s)$	Reference input
RCT	Robust control toolbox
$S(s)$	Sensitivity
SIMO	Single-input multi-output
SISO	Single-input single-output
$T(s)$	Complementary sensitivity

1.2. Introduction

In recent decades, researchers have dealt with precise position tracking of direct current (DC) servo motors. These motors are widely used in many practical applications due to their reliability, ability to handle large torques, fast response to input, and continuous operation without damage.

The researchers have studied many nonlinear control techniques in different applications, such as neuro-fuzzy control of DC motors [1], where a DC motor is employed as an actuator in the robotic manipulator. The DC servo motors have many applications in robots, airships, aircraft, and twin rotors. In each above application, the precise position tracking of the DC servo motor is required.

Predictive control of brushless DC motors in an automated process is achieved utilizing a generalized algorithm presented in [2]. Similarly, a nonlinear sliding mode control [3] of an actuator in robot application [4] is applied for obtaining precise results. Many other applications include nonlinear servo control for electric machines [5], stability analysis of servo control of DC motor drive, complete adaptive control of DC servo motors [6], speed control of DC servo systems using nonlinear sliding models, and nonlinear feedback control of series-connected DC motors [7]. Additionally, sliding mode optimal fuzzy [8], adaptive sliding mode fuzzy [9,10], and motion [11,12] controllers are nonlinear techniques that have been proposed.

Linear controllers are easy to implement in comparison to nonlinear controllers [13]. When conventional linear controllers are applied to nonlinear systems, the performance of linear control systems is degraded [14]. Simple structures and gains-based linear controllers have been used in many practical and industrial applications, such as simple proportional-integral-derivative (PID) control [15]. PIDs are one of the most common types of linear controllers, which have been employed for decades because of their low cost and simple, practical structure. However, in practice, the performance of these controllers is degraded when systems contain nonlinear characteristics. Conventional PID controllers do not provide the desired transient and steady-state specifications when a system contains nonlinearities or disturbance effects due to environmental conditions. Many advanced optimal and intelligent optimization techniques have been considered by researchers, such as optimized tuning [16], genetic algorithms (GAs), and metaheuristics [17], for optimal calculation of linear controllers and to improve the performance in real-time applications.

Compared to traditional PID controllers, fractional-order PID controllers produce better outcomes [18]. Nevertheless, their design requires optimizing five parameters, two of which are fractional derivative-order and integral-order parameters. The design entails solving five equations, and the optimization complexity is particularly noteworthy, primarily due to the fractional order.

The conventional robust H_2 and H_∞ controllers are designed based on the theory of hardy space of matrix-value functions, that is, H-infinity (H_∞) [19,20], and H_∞ loop shaping in the frequency domain [21–23]. With conventional and unstructured representation, these controllers achieve optimal and robust results [24]. These conventional robust controllers provide better transient and steady-state performances than traditional PID controllers. However, conventional H_∞ controllers have constraints on their structure order and response speed [25]. Moreover, due to their complex and high-cost hardware structure, conventional H_∞ controllers are less used for real-time applications in the industry.

The existing literature provides studies on conventional H_∞ control of DC servo motors and alternating current (AC) motors [26,27]. Transient and steady robust performance is achieved at the cost of the complex and higher-order structures of these conventional controllers. In an existing work on conventional H_∞ controllers [28], the authors selected second-order weights for their optimization. This work considered a fourth-order controller for the DC servo motor. In addition, the authors of [29] selected first-order weights to optimize a third-order conventional H_∞ controller.

The conventional H_∞ controllers are linear and the sliding mode controllers are nonlinear. The structure of these controllers depends on the selection of shaping weights. Due to the higher-order and complex structure, hardware implementation of conventional H_∞ controllers are hard and costly. Then, one can use a fixed-structure linear fraction transformation (LFT)-based H_∞ control architecture. This architecture is designed in the frequency domain by shaping closed-loop and complementary sensitivities with complex weights to obtain a robust, fast, transient, and steady-state behavior of the system.

The order of the fixed-structure H_∞ controller is independent of the order of complex weighting filters. The fixed structure $_\infty$ controller is of second-order and whose order is not affected by the selection of shaping weights. These frameworks can be represented as fixed-structure non-smooth H_∞ optimization problems [30,31]. The fractional transformation-based intelligent H_∞ controllers are more practical due to their simple structure and fixed order. Now, researchers have enhanced their focus on intelligent non-smooth H_∞ optimization. Many researchers use the GA-based intelligent approach to optimize the results of H_∞ controllers in different applications [32–34]. Another intelligent technique is the particle swarm optimization (PSO) [35], which is considered more effective in producing optimal results in H_∞ control problems [36,37]. The mayfly algorithm-based optimization [38] is helpful for the robust and optimal design of fixed-structure H_∞ synthesis. The corresponding tunable parameters may be optimized utilizing a novel mayfly algorithm, which is an advanced form of the PSO [35].

The fractional transformation-based intelligent H_∞ controller of a DC servo motor proposed in the present investigation is describes next. The fixed-structure intelligent, robust controllers are linear and their design requires a linear model of a DC servo motor. Therefore, first, one can derive the DC servo motor's linear time-invariant (LTI) model. Then, based on this LTI model, one may implement the linear intelligent, robust controller with a fixed structure and fixed order computationally; for example, by using `MATLAB` [39]. The linear control elements of the analyzed problem can be parameterized by using a non-smooth H_∞ optimization with the help of an intelligent, robust mayfly algorithm in `MATLAB`. These control elements are optimal and robust with a fixed-structure LFT objection function.

1.3. Contributions and Plan of the Article

Our contributions are given in Table 2. The remaining part of this article is organized as follows: Section 2 presents the mathematical modeling of DC servo motors. In Section 3, we introduce the intelligent fixed-structure and fixed-order H_∞, the conventional H_∞,

and traditional PID controllers. The comparison of the implemented three controllers by simulations is established in Section 4. The experimental results are provided in Section 5. Section 6 states the comparison and discussion for all three controllers. The transient specification is also boarded in Section 6, proving the effectiveness of the proposed fixed-structure H_∞ synthesis. The conclusions of the present investigation are provided in this section as well.

Table 2. Contributions of the present investigation.

Contribution	Description
1	While considering the cost and complexity issues of conventional robust H_∞ controllers, we design a decentralized and fixed-structure robust control system [40]. Thus, the proposed intelligent fixed-structure H_∞ controller overcomes the hardware cost and complexity limitations.
2	The fixed-structure H_∞ controller has not been investigated for precisely tracking the position of the DC servo motor.
3	The proposed controller is robust and linear with a fixed structure and fixed order.
4	Intelligent optimization of tunable parameters with one degree of freedom for the fixed-structure robust H_∞ control problem is another contribution to the proposed research. For this purpose, the proposed fixed-structure H_∞ for the control problem is formulated in `MATLAB` with the help of the robust control toolbox [39].
5	The proposed intelligent linear robust controller is also investigated on a real-time model of a DC servo motor. The performance of the proposed controller is compared with PID and conventional H_∞ controllers in terms of transient specifications, such as rise time, settling time, steady-state error, overshoot, and peak time.

2. Mathematical Modelling

2.1. Description of the DC Servo Motor

The DC servo module consists of a DC motor, tacho generator, gearbox with backlash, inertia load, magnetic breaks, and output disk connected with a gearbox and encoder. This servo mechanism is available at our laboratory, where a chain of modules starts with a tacho generator connected to a DC motor and ends with a gearbox. The potentiometer is placed outside the servo mechanism chain. The encoder measures the angle of the shaft's rotation of the DC motor. The voltages are produced by a tacho generator, which is directly proportional to the angular velocity of the DC motor. For this purpose, the tacho generator is directly connected to the DC motor. To implement the proposed control algorithm, the servo mechanism is interfaced with `MATLAB` as the proposed synthesis is linear and requires a mathematical model of the DC motor.

2.2. Mathematical Model of the DC Servo Motor

Nonlinear control applications require only a nonlinear model of a DC motor. Different nonlinear characteristics can be considered, such as the field flux $\varnothing_f(i_a)$, where f represents the magnetization curve and i_a is the armature current. Then, the nonlinear model is written as [7]

$$\frac{\mathrm{d}(L_a i_a + \varnothing_f(i_a))}{\mathrm{d}t} = -R_a i_a - K_a \varnothing_f(i_a)\omega + v_a, \quad (1)$$

$$J_m \frac{\mathrm{d}\omega}{\mathrm{d}t} = K_a \varnothing_f(i_a) i_a - D\omega - \tau_L, \quad (2)$$

where the notations stated in (1) and (2) are the following: L_a is the armature inductance, R_a is the armature resistance, K_a is the armature field constant, v_a is the armature input

voltage, J_m is the moment of inertia, ω is the angular velocity, τ_L is the load torque, D is the friction coefficient, and $e_b(t) = K_a \varnothing_f(i_a)\omega$ is the back electromotive force (EMF) that indicates the nonlinear behavior. The term $\tau_m = K_a \varnothing_f(i_a) i_a$ represents the torque produced by the motor. A linearized model of the DC motor is required for the proposed synthesis. After designing this synthesis for a linear model, the controller can be evaluated on a real-time model in the presence of all nonlinear characteristics. The first linear differential equation on the electrical side of Figure 1 and the linearized mathematical model for the DC servo motor are derived as

$$v_a(t) = R_a i_a(t) + L_a \frac{\mathrm{d}i_a(t)}{\mathrm{d}t} + e_b(t). \tag{3}$$

The second linear differential equation on the mechanical side of Figure 1 is written as

$$\tau_m(t) = J_m \frac{\mathrm{d}^2\theta(t)}{\mathrm{d}t^2} + \beta_m \frac{\mathrm{d}\theta(t)}{\mathrm{d}t}. \tag{4}$$

In the formulations stated in (3) and (4), the mechanical variables are related to the electrical variables as

$$\tau_m(t) = K_t\, i_a(t), \tag{5}$$

$$e_b(t) = K_b \frac{\mathrm{d}\theta(t)}{\mathrm{d}t}, \tag{6}$$

where K_t is the torque constant and K_b is the constant of back EMF.

Note that the above differential equations are expressed in the transfer function form as

$$V_a(s) = R_a\, I_a(s) + L_a s I_a(s) + E_b(s), \tag{7}$$

$$T_m(s) = J_m\, s^2\theta(s) + \beta_m s\theta(s), \tag{8}$$

$$T_m(s) = K_t\, I_a(s), \tag{9}$$

$$E_b(s) = K_b s\theta(s), \tag{10}$$

which are the transfer function representations of the expressions given in (3)–(6), respectively, assuming that the initial conditions are equal to zero. The angular velocity of the DC motor shaft is the first derivative of the angular position of the DC motor. Three methods may control the angular velocity, or angular position of the DC motor [41], which are summarized in Table 3.

Table 3. Control methods for the DC motor.

Method	Description
Armature control	The angular velocity or position of the DC motor is controlled by varying the armature resistance.
Flux control	The flux variation is controlled by adding the resistance parallel to the armature of the DC motor.
Input voltage control	The input voltage to the armature of the DC servo motor is varied to control the angular velocity or position of the shaft.

The final closed-loop transfer function is achieved by solving the equations presented in (7)–(10). The block diagram representation of the DC motor model is given in Figure 1.

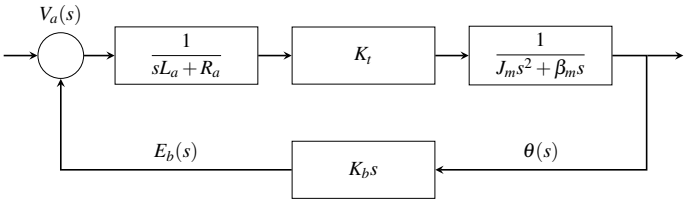

Figure 1. Block diagram of the DC motor.

Now, the feedback rule is applied to the block diagram in Figure 1 to achieve the final transfer function between the input voltage and output angular position. This rule is stated as

$$\frac{\theta(s)}{V_a(s)} = \frac{K_t}{L_a\ J_m\ s^3 + (R_a\ J_m + \ L_a\ B_m)s^2 + (R_a\ B_m + K_b\ K_t)s}. \tag{11}$$

In terms of s, we have that

$$\theta(s) = \frac{\omega(s)}{s}. \tag{12}$$

Replacing (12) in (11), we obtain the transfer function between the input voltage and output angular velocity of the shaft of the DC motor by means of

$$\frac{\omega(s)}{V_a(s)} = \frac{K_t}{L_a\ J_m\ s^2 + (R_a\ J_m + \ L_a\ B_m)s + (R_a\ B_m + K_b\ K_t)}.$$

Hence, the specific model of the DC motor, which is available in the laboratory of our university [42], is shown in Figure 2. The description of the variables can be seen in Table 4.

Table 4. Interpretation of the variables presented in Figure 2.

Variable	Description
$v_a(t)$	Input voltage.
$i_a(t)$	Armature current.
$\theta(t)$	Angular position.
$\omega(t)$	Angular velocity.
R_a	Armature resistance.
J_m	Inertia moment.
β_m	Damping coefficient.
$e_b(t)$	Back EMF.
$\tau_m(t)$	Electromechanical torque.

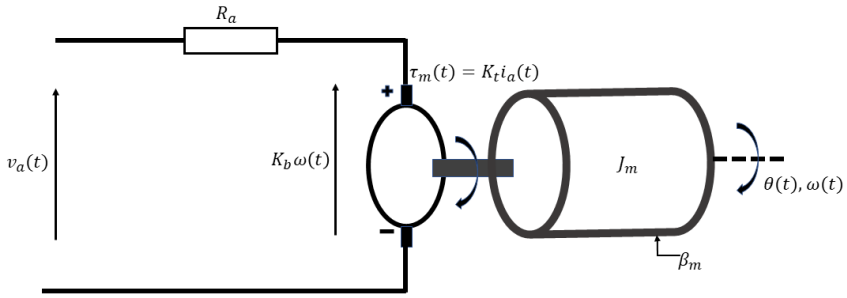

Figure 2. Linear model of the DC motor available in the laboratory.

The mechanical and electrical formulas are stated as

$$v_a(t) = R_a\ i_a(t) + \ K_b\omega(t), \tag{13}$$
$$J_m\dot{\omega}(t) = K_t\ i_a(t) - \beta_m\ \omega(t). \tag{14}$$

Note that the static kinetic friction of the model presented in (13) and (14) is linear, where the saturations are neglected. The first-order inertial system is obtained with the combination of electrical and mechanical formulations. Here, the inertial system is given by

$$T_s\ \dot{\omega}(t) = -\omega(t) + K_{sm}\ v(t), \tag{15}$$

where T_s is the time constant of the DC motor and K_{sm} is the motor gain. Both constants, T_s and K_{sm}, are defined as $T_s = (R_aJ_m)/(\beta_mR_a + K_bK_t)$ and $K_{sm} = K_m/(\beta_mR_a + K_bK_t)$.

In the frequency domain, the expression formulated in (15) becomes

$$T_s[s\omega(s)] = -\omega(s) + K_{sm}v(s). \tag{16}$$

From (16), we define the transfer functions, which are stated as

$$G_{P1}(s) = \frac{\omega(s)}{v(s)} = \frac{K_{sm}}{sT_s+1}, \tag{17}$$

$$G_{P2}(s) = \frac{\theta(s)}{v(s)} = \frac{K_{sm}}{s(sT_s+1)}. \tag{18}$$

The transfer function between angular velocity and the input voltage is given in (17), whereas the transfer function between the angular position and the input voltage is provided in (18).

The pulse-width modulation (PWM) signal is applied as the control signal to the DC servo motor. The input signal $v(t)$ is scaled as $u(t) = v(t)/v_{\max}$, which satisfies the condition $|u(t)| \leq 1$. By defining $K_s = K_{sm}v_{\max}$, the final transfer functions for the angular velocity and position as outputs are presented as

$$\widehat{G}_{P1}(s) = \frac{\omega(s)}{u(s)} = \frac{K_s}{sT_s+1}, \tag{19}$$

$$\widehat{G}_{P2}(s) = \frac{\theta(s)}{u(s)} = \frac{K_s}{s(sT_s+1)}, \tag{20}$$

with the notations used in (19) and (20) being established as above.

2.3. State-Space Model Equations of the DC Servo Motor

Two state variables are defined for representing the model in state-space form. The state vector contains two state variables, which we see in Table 5.

Table 5. Interpretation of variables in the DC servo motor mathematical model.

Variable	Description
x_1	Angle θ in radians (rad), which determines the angular shaft position.
x_2	Velocity ω in rad/sec, which represents the angular shaft velocity.

From (15), we have

$$\begin{aligned} T_s\dot{\omega}(t) &= -\omega(t) + K_{sm}(v_{\max}u(t)), \\ T_s\dot{\omega}(t) &= -\omega(t) + K_s\, u(t), \\ \dot{\omega}(t) &= \left(\frac{-1}{T_s}\right)\omega(t) + \left(\frac{K_s}{T_s}\right)u(t). \end{aligned} \tag{21}$$

The system of differential equations that is obtained from (21) for the LTI state-space model is given by

$$\dot{x_1} = x_2 \tag{22}$$

$$\dot{x_2} = ax_2 + bu, \tag{23}$$

where $a = -1/T_s < 0$ and $b = k_s/T_s > 0$. The final single-input multi-output (SIMO) state-space model is established as

$$\begin{bmatrix} \dot{x_1} \\ \dot{x_2} \end{bmatrix} = \begin{bmatrix} 0 & 1 \\ 0 & -\frac{1}{T_s} \end{bmatrix} \begin{bmatrix} x_1 \\ x_2 \end{bmatrix} + \begin{bmatrix} 0 \\ \frac{k_s}{T_s} \end{bmatrix} u. \tag{24}$$

The matrix representation expressed in (22) and (23) is formulated in (24). The linear model stated in (24) is unstable for the open-loop step response of the angular position. The parameter values of the laboratory servo mechanism are estimated experimentally, where the DC motor is connected to the tacho generator, inertia load, gearbox, and output disk. The estimated parameter values are provided in Table 6. We can see the open-loop `Simulink` model in Figure 3. Similarly, in Figure 4, the closed-loop `Simulink` model is displayed. This closed-loop `Simulink` model is developed with unity gain as a controller in the feedforward path to the DC servo motor in a negative feedback closed-loop system. In addition, the input voltage, open-loop step response for the angular position, and open-loop step response for the angular velocity are given in Figures 5 and 6, respectively. Additionally, Figure 7 shows the closed-loop step response for the position and velocity. The closed-loop model, the expression stated in (23) is replaced by $\dot{x_2} = ax_2 + bu - bx_1$.

Table 6. Values of experimentally estimated parameters for a DC servo motor.

Symbol	Values	Units
$v_{\max}$	12.00	V
T_s	1.04	sec
K_s	186.00	rad/sec
a	−0.96	seg^{-2}
b	178.80	rad/seg^2

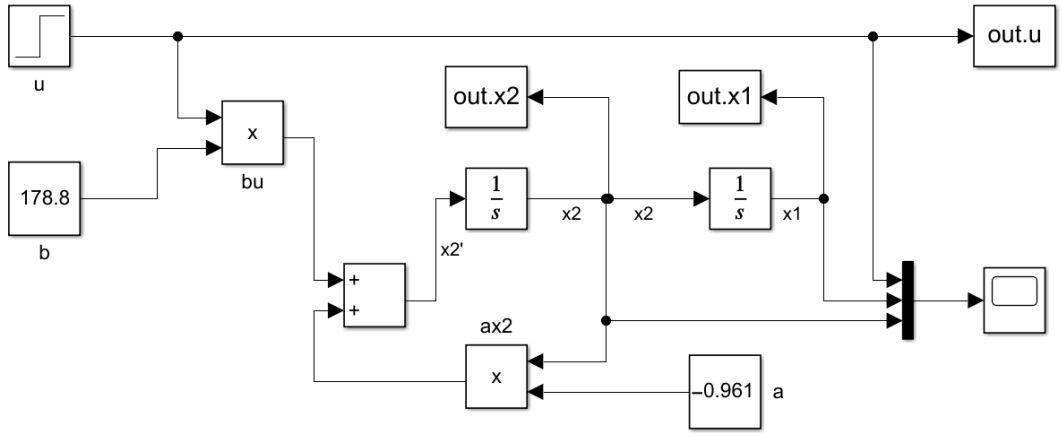

Figure 3. Open-loop `Simulink` model of the DC servo motor.

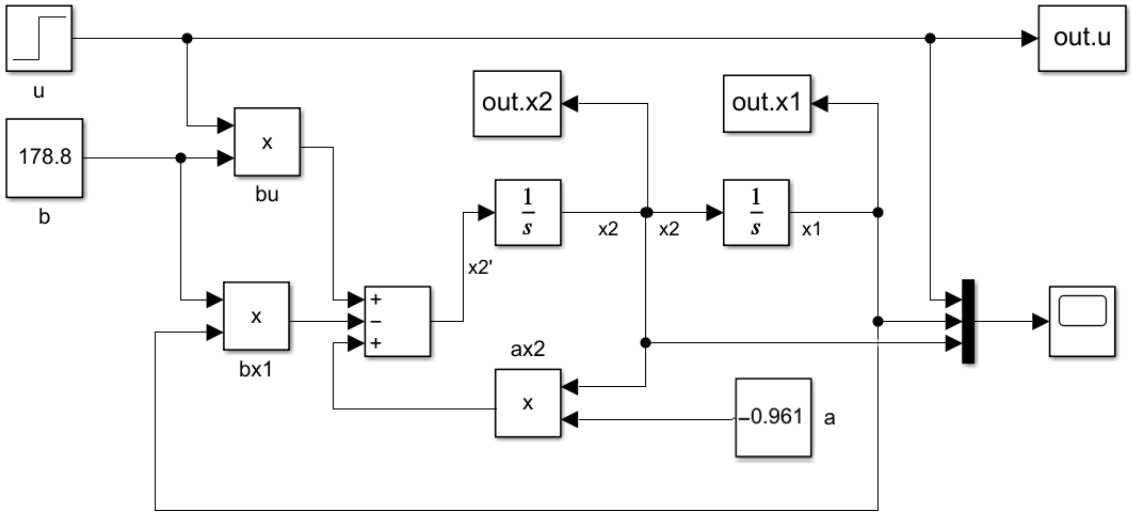

Figure 4. Closed-loop `Simulink` model for position tracking of the DC servo motor.

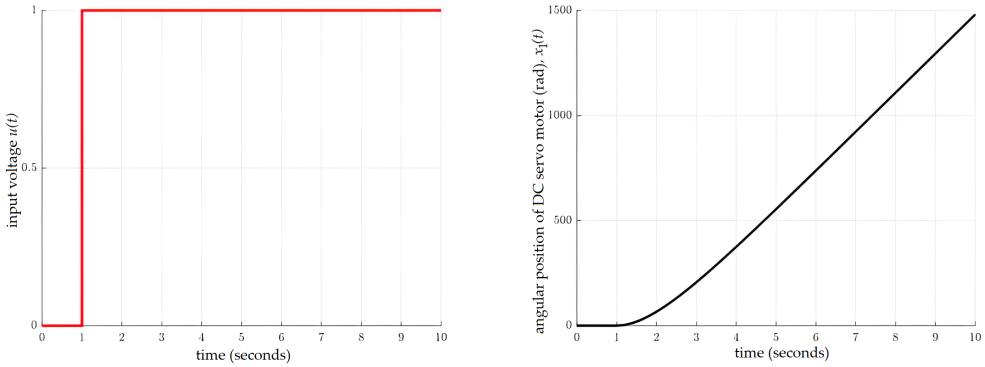

(a) **(b)**

Figure 5. Input voltage (**a**) and open-loop step response for position (**b**) of the DC servo motor.

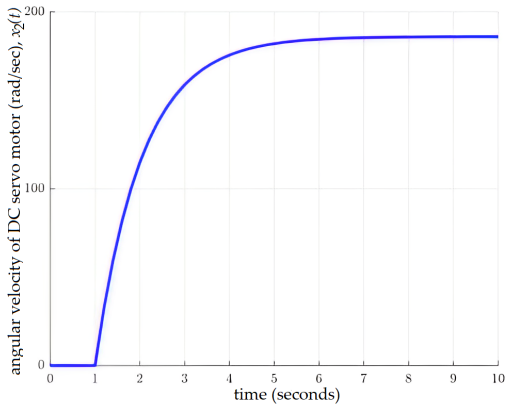

Figure 6. Open-loop step response for velocity of the DC servo motor.

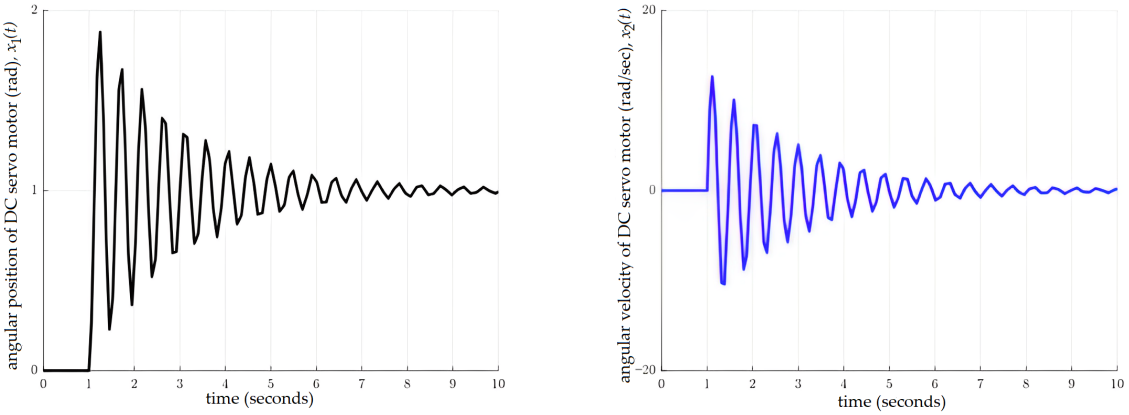

(**a**) (**b**)

Figure 7. Closed-loop step response for position (**a**) and velocity (**b**) of the DC servo motor.

3. Design of Controllers for a DC Servo Motor System

3.1. PID Controller

In recent decades, the PID controllers were designed with standard techniques such as the root locus, pole-zero placement, and Ziegler–Nichols methods. These controllers are widely used in many control applications, and their implementation is simple. If the systems are nonlinear, the performances of these controllers become poor. Such controllers do not conduct well with environmental disturbances because of their conventional design. A traditional PID controller was designed using the Ziegler–Nichols method [43].

The values of the tuned parameters K_p, K_i, and K_d of PID controllers are provided in Table 7. We compare the traditional PID controllers according to their transient specifications and commanded signal tracking. The expressions that govern the behavior of a traditional PID controller are described as

$$u(t) = K_p e(t) + K_i \int_0^t e(\tau)\mathrm{d}\tau + K_d \frac{\mathrm{d}e(t)}{\mathrm{d}t}, \quad (25)$$

$$U(s) = \left(K_p + \frac{K_i}{s} + sK_d\right) E(s), \quad (26)$$

where the formula presented in (26) is obtained by applying the Laplace transform to (25), assuming that $e(0) = 0$, where here "s" is the Laplace variable.

Table 7. Tuned parameters of PID controllers using the Ziegler–Nichols method for angular tracking.

Symbol	Description	Value
K_p	Proportional gain	0.1405
K_i	Integral gain	0.0305
K_d	Derivative gain	0.0240

3.2. Design of the Conventional H_∞ Controller

The design of a conventional H_∞ controller is based on filters shaping the open-loop or closed-loop frequency responses. This controller is designed in the frequency domain. The complex weights shape the closed-loop sensitivity $S(s)$ and complementary sensitivity $T(s)$. Thus, with the selection of suitable complex weights on $S(s)$ and $T(s)$, the H_∞ norm is reduced. This norm is the main constraint on this conventional controller's robust structure, bandwidth, and transient specifications. Its formulation is known as the H_∞ optimal control problem [44]. The constraints to optimize the controller parameters are given by

$$\|w_s(s)S(s)\|_\infty \leq 1, \ \|w_T(s)T(s)\|_\infty \leq 1. \quad (27)$$

The constraints stated in (27) provide a margin for robustness and a better disturbance and noise rejection over a range of frequencies. The H_∞ optimal control is also robust and provides better performance than the traditional PID. The MIXSYN tool is used to design this H_∞ optimal robust controller in `MATLAB`. The order of this controller is increased by utilizing the complex weight. The drawback, which reduces the practical importance, is the complexity of the structure of this synthesis. The calculated state-space structure of the 3rd-order H_∞ controller of DC servo motor is expressed as

$$A = \begin{bmatrix} -0.001 & 0 & 0 \\ 2.2 \times 10^7 & -2753 & -3.18 \times 10^9 \\ 0 & 0.001 & 0 \end{bmatrix}, B = \begin{bmatrix} 0.106 \\ 0 \\ 0 \end{bmatrix}, C = \begin{bmatrix} 1.62 \times 10^6 \\ -202.70 \\ -2.34 \times 10^8 \end{bmatrix}^\top, D = \begin{bmatrix} 0 \end{bmatrix}.$$

3.3. Design of the Proposed Intelligent Fixed-Structure H_∞ Controller

Conventional H_∞ controllers have a monolithic structure. Due to their complex structure, these controllers have not been used widely in industrial applications. Such controllers also have a constraint on their order. However, although they are robust, they are not suitable for many practical applications due to the mentioned constraints. These H_∞ controllers have a constraint on the H_∞ norm regarding the speed of response and robust bandwidth. To overcome the limitations of conventional PIDs and H_∞ controllers, the fixed-structure H_∞ control synthesis with intelligent optimization is proposed. These fixed-structure H_∞ controllers are robust and linear with a fixed order [45]. The standard form of the proposed fixed-structure control, with non-tunable and tunable blocks, is shown in Figure 8.

Next, we describe a standard formulation and a design of fixed-structure H_∞ synthesis using a mayfly optimization algorithm. This standard formulation is comprised of two parts: (i) the block $P(s)$ that is LTI, which is comprised non-tunable fixed blocks, and (ii) the second block that is comprised fixed-order control elements $C_i(s)$, where $i \in \{1, \ldots, N\}$ in diagonal form. This diagonal matrix, $\text{diag}(C_1(s), \ldots, C_N(s))$ namely, is used in MIMO systems. Each tunable control element $C_i(s)$ is LTI with a fixed order. The second block contains one control element in the case of single-input single-output (SISO) systems. Note that the single control element is robust and LTI.

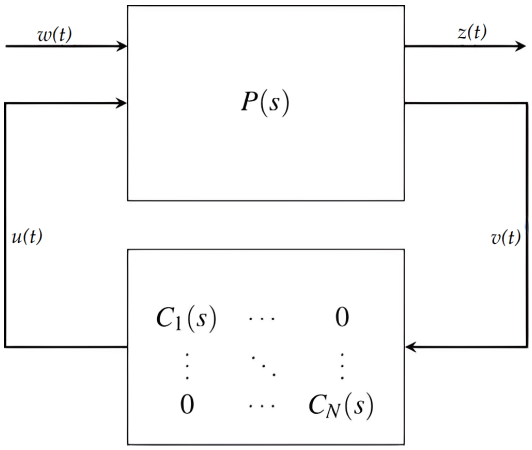

Figure 8. Standard formulation of the fixed-structured H_∞ synthesis.

According to the robust control theory, all the SISO or MIMO systems can be formulated into the standard form of Figure 8. The isolated tunable control elements exist in the lower block of Figure 8, where each of them has a defined structure in the case of MIMO systems. The non-tunable plant model is placed into block $P(s)$. Note that $P(s)$ and $C(s)$ are the transfer function representations of non-tunable and tunable blocks, respectively. This transfer function form is achieved by applying the Laplace transform to the time domain LTI equation. The external inputs are combined in w, such as disturbances and the commanded inputs. The variable $z(t)$ contains the error signal, such as $z(t) = y(t) - r(t)$, where $y(t)$ is the true output, and $r(t)$ is the reference input. Consider the matrix formulation given by

$$\begin{pmatrix} z(t) \\ v(t) \end{pmatrix} = P \begin{pmatrix} w(t) \\ u(t) \end{pmatrix} = \begin{pmatrix} P_{11} & P_{12} \\ P_{21} & P_{22} \end{pmatrix} \begin{pmatrix} w(t) \\ u(t) \end{pmatrix}. \tag{28}$$

The partition of (28) is the standard formulation of the fixed-structured LFT H_∞ synthesis. The LFT from $w(t)$ to $z(t)$ is $T_{wz}(s) = F_l(P, C) := P_{11} + P_{12}C(I - P_{22})^{-1}P_{21}$ or $H(s) = F_l(P(s), \text{diag}(C_1(s), \ldots, C_N(s)))$. The criterion on the fixed-structure LFT objective function for robust transient response is defined as

$$\begin{cases} f_o = t_s < 0.3\,\text{sec}\ (2\%\ \text{error criteria}); \\ f_1 = \sigma - 0\%\ (\text{percent overshoot}); \\ f_2 = \|F_l(P, C)\|_\infty < \gamma, \text{ where } \gamma = 1. \end{cases}$$

The next challenge is to achieve the defined objective criteria of the proposed fixed structure. The H_∞ problem is resolved using the mayfly approach, where the proposed intelligent procedure works as indicated in Algorithm 1. Four parameters of linear robust controllers, such as K_p, K_i, K_d, and T_f, are optimized by the above proposed intelligent fixed-structure H_∞ optimization employing $C_j(s) = K_p + K_i/s + K_d s/T_f s + 1$. These parameters

are tuned to fulfill the design requirements. The complex weights shape the closed-loop sensitivity $S(s)$ and complementary sensitivity $T(s)$.

Algorithm 1: Mayfly optimization approach

begin

Step 1: Initialize the shaping weights and tunable parameters of the fixed-structure synthesis as individuals, where they find positions $p_i(t)$ and velocities $v_i(t)$ for the current iteration as $p_i(t) = p_i(t) + v_i(t)$.

Step 2: Update the weighted distance using an expression stated as

$$v_i(t+1) = \begin{cases} gv_i(t) + a_1 \exp^{-\beta r_m^2}[x_i(t) - y_i(t)], \text{if } f(y_i) > f(x_i); \\ gv_i(t) + flr_1, \text{if } f(y_i) < f(x_i); \end{cases}$$

where g is the weighted current velocity, r_m is the Cartesian distance between them, r_1 is a random number, and other parameters are constants. The Cartesian norm of their positions is formulated as $\|x_i - y_i\| = (\sum_{k=1}^{n} (x_{ik} - y_{ik})^2)^{1/2}$. Note that after spending several years in water, at the end of their life, mayflies travel to their mate to reproduce with them. Female mayfly $y_i(t)$, with its little away mate $x_i(t)$, if $f(y_i) > f(x_i)$, will speed up to approach her male partner.

Step 3: Update their velocities according to the best global position x_g utilizing

$$v_i(t+1) = \begin{cases} gv_i(t) + a_2 \exp^{-\beta r_p^2}(x_{hi}(t) - x_i(t)) + a_3 \exp^{-\beta r_g^2}[x_{gi}(t) - x_i(t)], \\ \text{if } f(x_i) > f(y_i); \\ gv_i(t) + dr_2, \text{if } f(x_i) < f(y_i); \end{cases}$$

where r_g and r_p are the Cartesian distance between individual i and the best global position in the swarms to the best historical trajectory, respectively. Observe that male mayflies $x_i(t)$ tend to gather in swarms and will be stronger than their best fitness values based on their experiences.

Step 4: Mate the top half of male flies with the remaining half of female flies, producing offspring with their best fitness values, given as offspring1 $= r_0$ male $+ (1 + r_0)$ female and offspring2 $= r_0$ female $+ (1 + r_0)$ male, where r_0 represents a random number.

Step 5: Guarantee convergence, which is proposed using $v_i(t+1) = -x_i(t) + x_{hi} + gv_i(t) + \rho(t)(1 - 2r_3)$, where r_3 represents a random number generated from the Gaussian distribution.

end

4. Comparison of Simulation Results for the Three Controllers

4.1. Setting

The optimized parameters of the proposed controller make the overall system robust in the case of plant parameter uncertainty and also provide improved transient specifications compared to the other two conventional controllers. The optimized parameter values are given in Table 8.

Table 8. Values of the optimized parameters for structure H_∞ synthesis for angular position tracking.

Symbol	Description	Value
K_p	Proportional gain	0.0806
K_i	Integral gain	1.17×10^{-8}
K_d	Derivative gain	0.086
T_f	1st order differential coefficient	0.000129

4.2. The Conventional Controllers

The performance comparison between all three controllers for different reference inputs is reported in Table 9. Figure 9a,b represent step input tracking and square input tracking, respectively. Figure 10 shows the control effort comparison for all three controllers for tracking a square input, whereas Figure 11 displays the disturbance rejection comparison of all three controllers. Figure 12 provides the robust performance of the proposed controller

in the presence of model uncertainty (a) and the proposed synthesis performance for the model uncertainty (b).

Table 9. The performance comparison between proposed and conventional controllers.

Controller	Controller Order	Rise Time (sec)	Settling Time (sec)	Over-Shoot (%)	Steady-State Error
Traditional PID		0.25	2.5	24.2	0%
Conventional H_∞	3rd	0.20	0.35	0	0%
Intelligent fixed-structure H_∞	2nd	0.18	0.33	0	0%

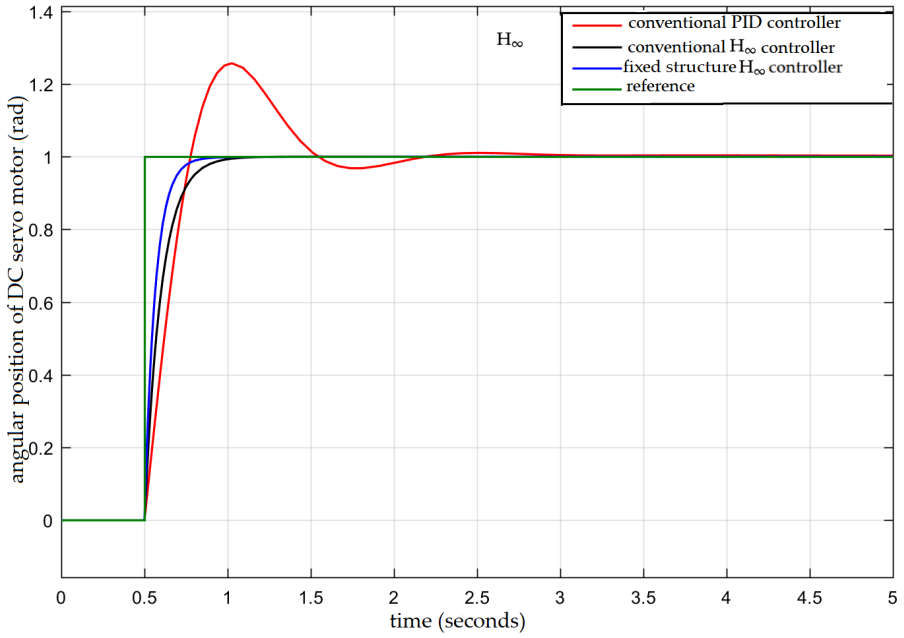

(**a**)

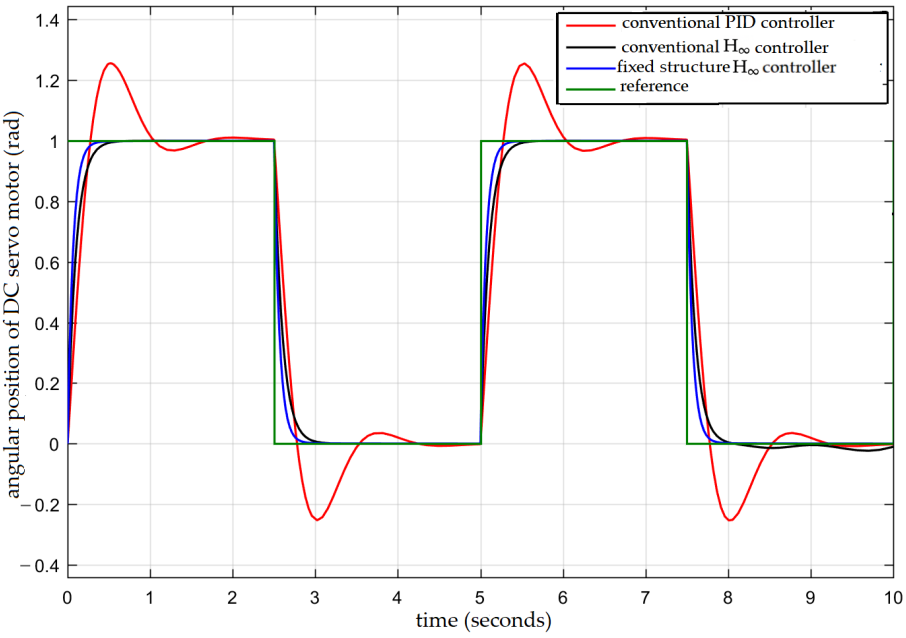

(**b**)

Figure 9. Step input tracking (**a**) and square input tracking (**b**).

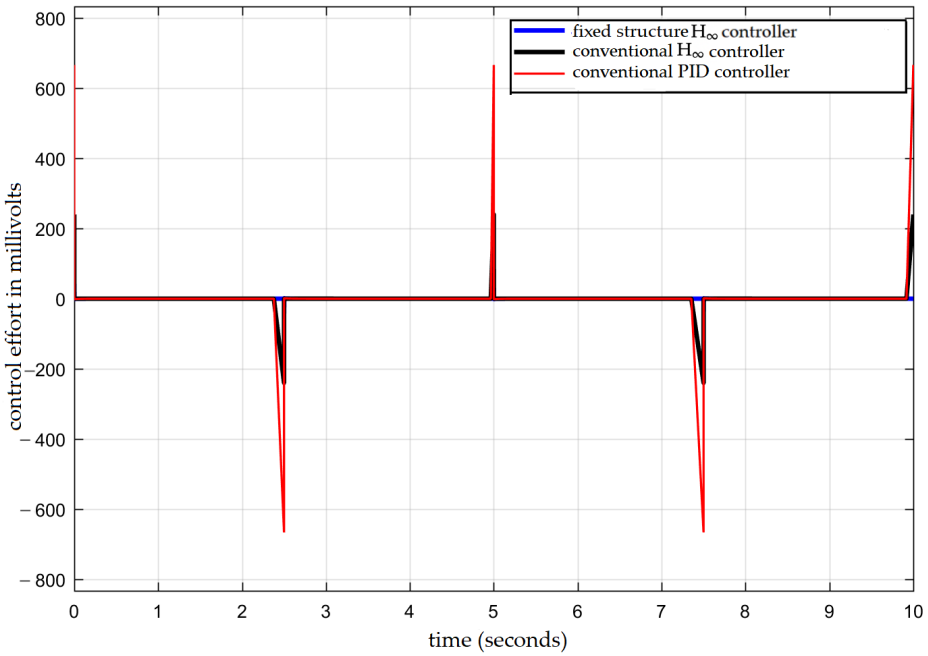

Figure 10. Control effort of all three controllers for angular position tracking (square input tracking as shown in Figure 9b).

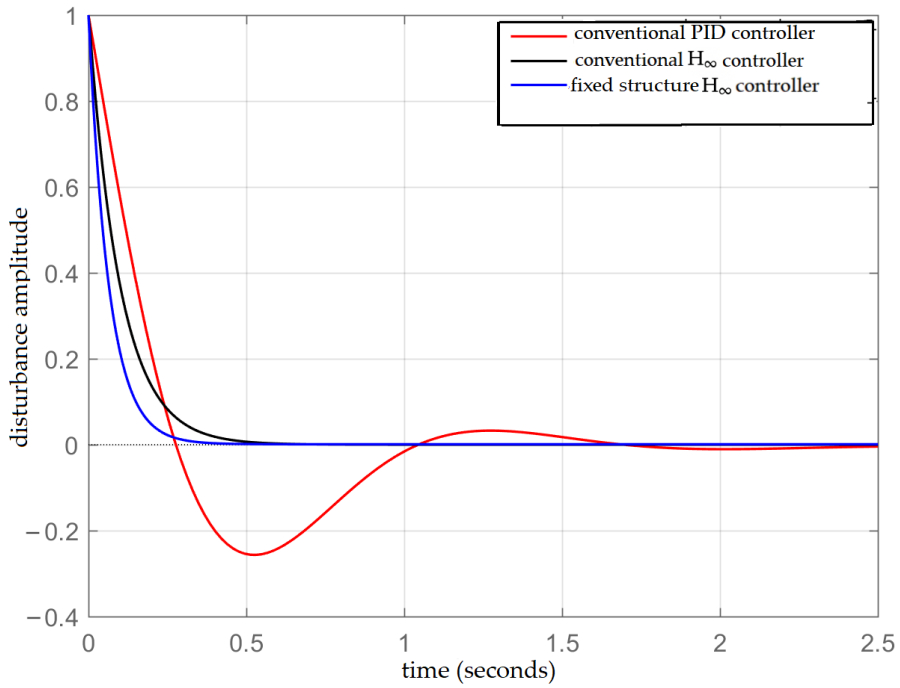

Figure 11. Step disturbance rejection comparison among all three controllers.

4.3. The Proposed Controller

The proposed controller response is plotted in Figure 12 with its parametric uncertainties (range of variations), which shows the robustness of the controller response, that is, the controller performance is maintained despite variations. Because this is a robust controller, a range of parameter variations are tested to validate its robustness. Then, the corresponding open-loop and closed-loop responses are plotted.

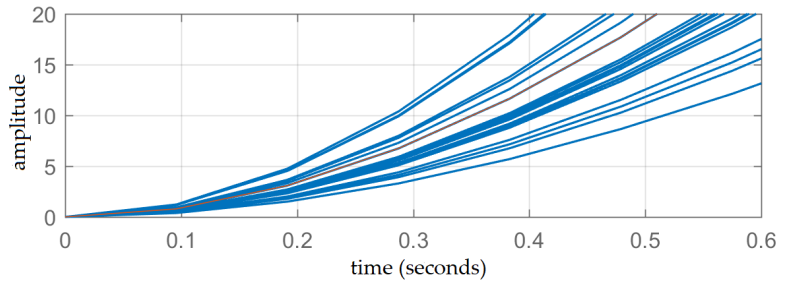

(**a**)

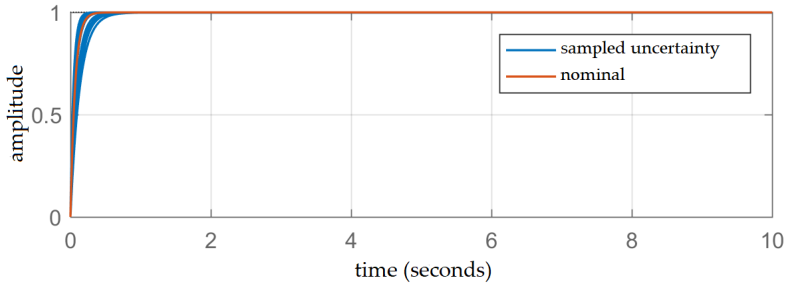

(**b**)

Figure 12. Plant's open-loop step in the presence of parametric uncertainty (**a**) and the proposed synthesis performance for the model's uncertainty (**b**).

5. Experimental Setup and Results

5.1. Experimental Setup for a DC Servo Motor

The experimental setup of the DC servo mechanism available in the laboratory of our university is comprised of the modules that we can see in Table 10. The whole MSS setup is shown in Figure 13.

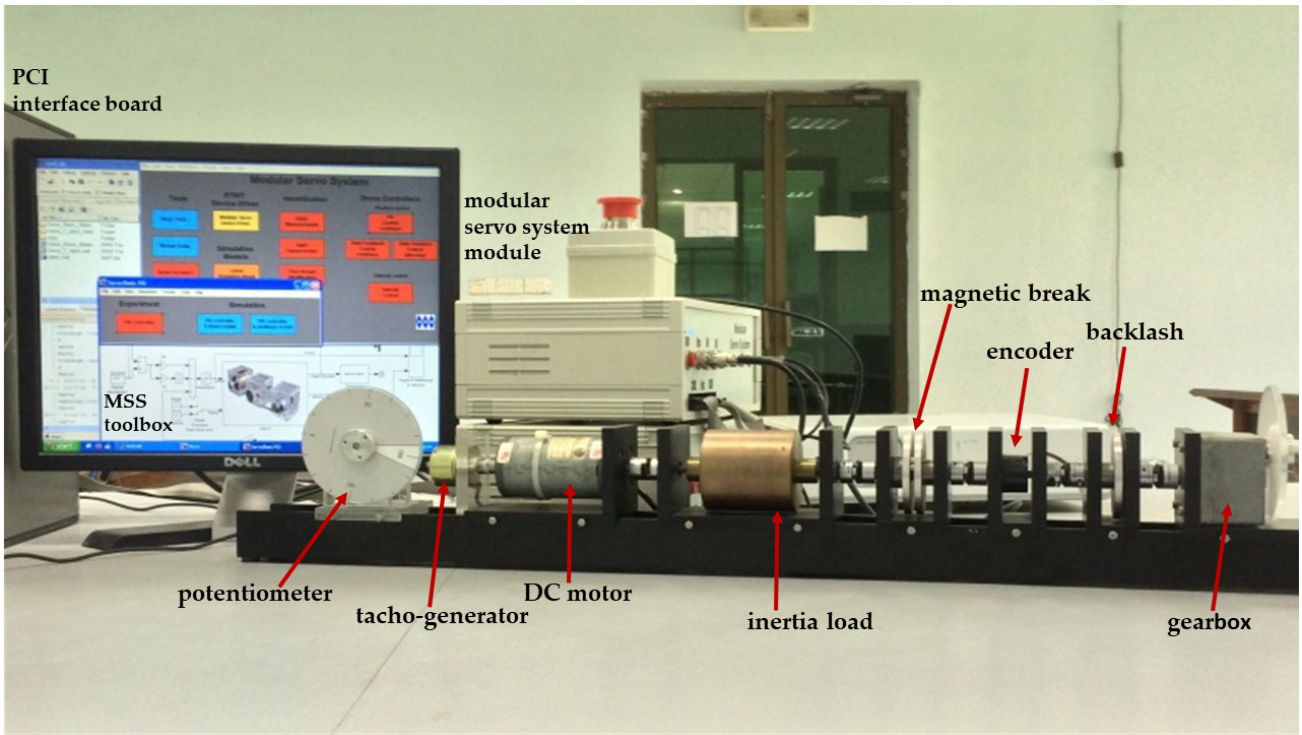

Figure 13. The experimental setup of the DC servo mechanism.

Table 10. Modules of the DC servo mechanism.

Module	Description
Tacho generator	Converter of mechanical energy into electrical energy. A tacho generator measures the angular shaft speed and provides output in the form of voltage proportional to the angular velocity.
Encoder	Measurer of the angular rotation of the DC motor. The potentiometer is connected outside the servo mechanism.
MSS	Connecter of backlash, magnetic brake, gearbox, and circular disk using the MSS inertia load in the chain.
MSS toolbox	Tool operated directly in the `Simulink` of `MATLAB` environment. This MSS toolbox has the excess of all the PCI/RTDAC acquisition board functions. The PCI board is equipped with an A/D converter, and the whole measurement system is based on this PCI board equipped with an A/D converter.
PCI board	Controller of angular speed and position of the DC motor. The PWM pulses are generated in an appropriate sequence. The DC motor is configured with PCI board and I/O board for communication purposes. The PCI board reads encoder signals and produces PWM pulses in the appropriate sequence to control the servo motor.

5.2. Results

The experiment results for the traditional PID and the proposed intelligent fixed-structure H_∞ are given in Figures 14 and 15, respectively. The discussion of these results is provided in the next section.

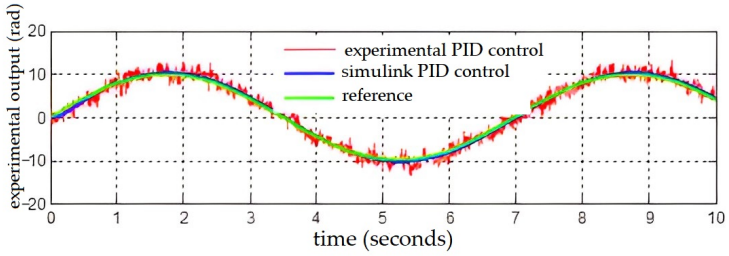

(**a**)

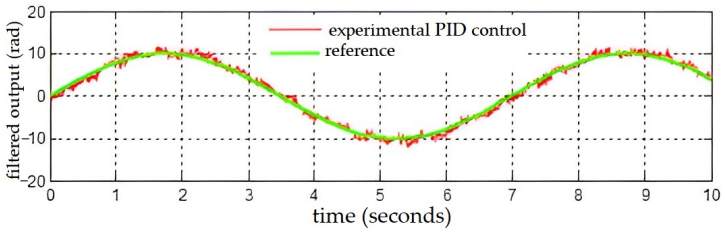

(**b**)

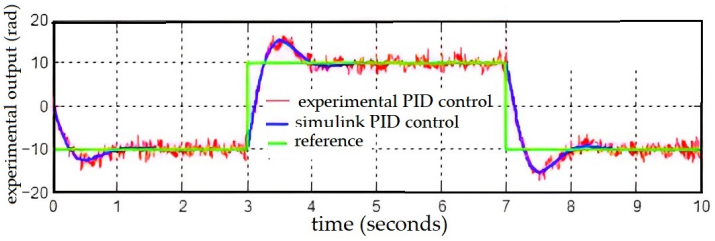

(**c**)

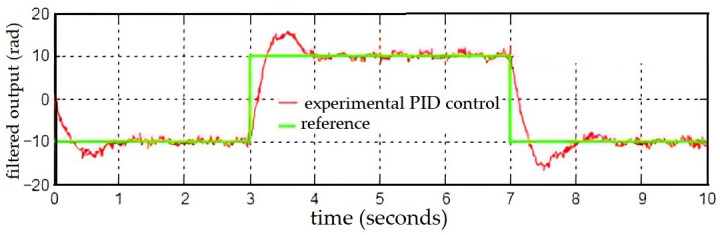

(**d**)

Figure 14. The experimental PID controller for angular position tracking—sine input tracking—(**a**,**b**) and the experimental PID controller for angular position tracking—square input tracking (**c**,**d**).

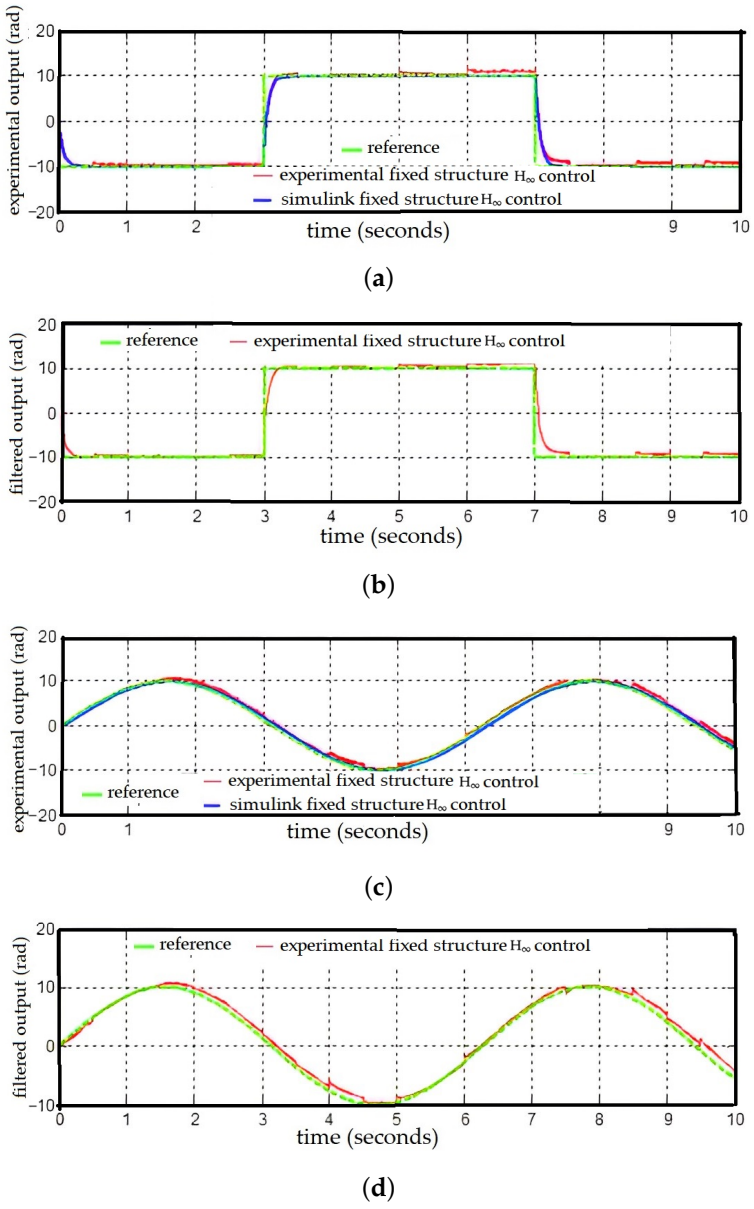

Figure 15. The experimental fixed-structure H_∞ controller for angular position tracking—square input tracking—(**a**,**b**) and the experimental fixed-structure H_∞ controller for angular position tracking—sine input tracking (**c**,**d**).

6. Comparison, Discussion, and Conclusions

6.1. Performance Comparison and Discussion

Next, we study the proposed intelligent fixed-structure H_∞ controller in real-time for precise position tracking of a DC servo motor. As mentioned, this DC servo motor is a compulsory part of many control systems; for example, its practical applications are in robotics, aircraft, and twin rotors, among others. The performance of these systems always depends upon the DC servo motor. Precise position tracking of this motor with the desired transient specifications is challenging. As mentioned, although conventional PID controllers are low-cost and have a simple structure, their design using traditional techniques does not provide the desired transient specifications in many systems. The conventional H_∞ optimal controllers perform better than the standard PID controllers.

In the case of higher-order systems, the structure of the conventional H_∞ controllers becomes complex. These controllers have limitations on their practical applications due to this complex structure. The proposed fixed-structure H_∞ controllers are robust and have a very simple fixed structure. Because the proposed controller for the DC servo motor has a similar structure to that of conventional PID, its hardware implementation requires operational amplifiers for parallel implementation of integral, derivative, and simple gain actions. As the parameters of the proposed controller are optimized intelligently, some computational costs are incurred while keeping the fixed structure of such controller. The order of this controller is independent of the complex weights used to shape $S(s), T(s)$.

The parameters of the LTI structured control elements are optimized by intelligent algorithms while fulfilling the H_∞ condition. The proposed linear robust controller has provided good experimental results. Additionally, the performance comparison presented in Table 9 between the proposed and conventional controllers has proved that our proposal gives better transient specifications than conventional controllers.

6.2. Conclusions

The DC servo motor is the functional part of many practical systems, such as twin rotors, airships, aircraft, and robot manipulators. Precise angular position tracking with the best transient specifications is a big challenge. The proposed intelligent fixed-structure H_∞ synthesis has proved its practical importance by means of experimental results. The main advantage of this controller is its simple structure and fixed order. The conventional H_∞ controller is also robust and gives better transient specifications than the traditional PID controller. However, practical use of the conventional H_∞ controller is limited due to its complex structure. The order of the conventional H_∞ controller is the sum of the complex weighting filters and the plant's order. Due to this reason, the structure of the conventional H_∞ controller becomes more complex in the case of higher-order systems. Thus, the employment of conventional H_∞ controllers in practice is limited. Note that the order of the proposed controller is not affected by complex weighting filters. Because of the reasons above, the practical use of our robust controller is simple, and the hardware and computational costs are also meager. The parameters of the fixed-structure H_∞ synthesis are optimized by intelligent non-smooth algorithms to handle the plant parameters' dynamic behavior and provide robust stability in the case of parameter uncertainty. The proposed fixed-structure H_∞ controllers are effective for both MIMO and SISO systems. As the DC servo motors are the compulsory part of many hybrid systems, the idea for future research is that the proposed approach can also tune the decentralized controllers of such hybrid and MIMO systems to reduce the complexity of complex MIMO systems. In addition, a plant input saturation may lead to the integral windup phenomenon in the system. The elimination of this phenomenon will require an anti-integral windup control strategy in addition to the proposed control strategy, which will be further investigated.

Author Contributions: Conceptualization, M.Z.U.R., V.L. and C.M.-B. Formal analysis, M.Z.U.R., V.L. and C.M.-B. Investigation, M.Z.U.R., V.L., C.M.-B., I.M., M.U. and M.R. Methodology, M.Z.U.R., V.L., C.M.-B., I.M., M.U. and M.R. Writing—original draft, M.Z.U.R., C.M.-B., I.M., M.U. and M.R. Writing—review and editing, V.L. All authors have read and agreed to the published version of the manuscript.

Funding: This research was funded partially by project grant Fondecyt 1200525 (V.L.) from the National Agency for Research and Development (ANID) of the Chilean government under the Ministry of Science, Technology, Knowledge and Innovation.

Institutional Review Board Statement: Not applicable.

Informed Consent Statement: Not applicable.

Data Availability Statement: Not applicable.

Acknowledgments: The authors would also like to thank four reviewers for their constructive comments which led to improve the presentation of the manuscript.

Conflicts of Interest: There are no conflict of interest declared by the authors.

References

1. Wai, R.J.; Chen, P.C. Robust neural-fuzzy-network control for robot manipulator including actuator dynamics. *IEEE Trans. Ind. Electron.* **2006**, *53*, 1328–1349. [CrossRef]
2. Low, K.S.; Chiun, K.Y.; Ling, K.V. Evaluating generalized predictive control for a brushless DC drive. *IEEE Trans. Power Electron.* **1998**, *13*, 1191–1198.
3. Alshammari, O.; Kchaou, M.; Jerbi, H.; Aoun, S.B.; Leiva, V. A fuzzy design for a sliding mode observer-based control scheme of Takagi-Sugeno Markov jump systems under imperfect premise matching with bio-economic and industrial applications. *Mathematics* **2022**, *10*, 3309. [CrossRef]
4. Wai, R.J.; Muthusamy, R. Fuzzy-neural-network inherited sliding-mode control for robot manipulator including actuator dynamics. *IEEE Trans. Neural Netw. Learn. Syst.* **2012**, *24*, 274–287.
5. Dawson, D.M.; Hu, J.; Burg, T.C. *Nonlinear Control of Electric Machinery*; CRC Press: New York, NY, USA, 2019.
6. Sevinc, A. A full adaptive observer for DC servo motors. *Turk. J. Electr. Eng. Comput. Sci.* **2003**, *11*, 117–130.
7. Mehta, S.; Chiasson, J. Nonlinear control of a series DC motor: theory and experiment. *IEEE Trans. Ind. Electron.* **1998**, *45*, 134–141. [CrossRef]
8. Antić, D.; Milojković, M.; Jovanović, Z.; Nikolić, S. Optimal design of the fuzzy sliding mode control for a DC servo drive. *J. Mech. Eng.* **2010**, *56*, 455–463.
9. Sharkawy, A.B.; Salman, S.A. An adaptive fuzzy sliding mode control scheme for robotic systems. *Intell. Control Autom.* **2011**, *2*, 299–309. [CrossRef]
10. Charfeddine, S.; Alharbi, H.; Jerbi, H.; Kchaou, M.; Abbassi, R.; Leiva, V. A stochastic optimization algorithm to enhance controllers of photovoltaic systems. *Mathematics* **2022**, *10*, 2128. [CrossRef]
11. Akar, M.; Temiz, I. Motion controller design for the speed control of DC servo motor. *Int. J. Appl. Math. Inform.* **2007**, *1*, 131–137.
12. Liu, F.; Zhang, X. Compound adaptive fuzzy synchronization controller design for uncertain fractional-order chaotic systems. *Fractal Fract.* **2022**, *6*, 652. [CrossRef]
13. Ackermann, J.; Guldner, J.; Sienel, W.; Steinhauser, R.; Utkin, V.I. Linear and nonlinear controller design for robust automatic steering. *IEEE Trans. Control Syst. Technol.* **1995**, *3*, 132–143. [CrossRef]
14. Valluru, S.K.; Singh, M. Performance investigations of APSO tuned linear and nonlinear PID controllers for a nonlinear dynamical system. *J. Electr. Syst. Inf. Technol.* **2018**, *5*, 442–452. [CrossRef]
15. Dubey, S.; Srivastava, S.K. A PID controlled real time analysis of DC motor. *Int. J. Innov. Res. Comput. Commun. Eng.* **2013**, *1*, 1965–1973.
16. Mpanza, L.J.; Pedro, J.O. Optimised tuning of a PID-Based flight controller for a medium-scale rotorcraft. *Algorithms* **2021**, *14*, 178. [CrossRef]
17. Sabir, M.M.; Khan, J.A. Optimal design of PID controller for the speed control of DC motor by using metaheuristic techniques. *Adv. Artif. Neural Syst.* **2014**, *2014*, 126317. [CrossRef]
18. Muresan, C.I.; Birs, I.; Ionescu, C.; Dulf, E.H.; De Keyser, R. A review of recent developments in autotuning methods for fractional-order controllers. *Fractal Fract.* **2022**, *6*, 37. [CrossRef]
19. Lien, C.H.; Chang, H.C.; Yu, K.W.; Li, H.C.; Hou, Y.Y. Robust H∞ controller design of switched delay systems with linear fractional perturbations by synchronous switching of rule and sampling input. *Fractal Fract.* **2022**, *6*, 479. [CrossRef]
20. Doyle, J.; Glover, K.; Khargonekar, P.; Francis, B. State-space solutions to standard H_2 and H_∞ control problems. In Proceedings of the 1988 American Control Conference, Atlanta, GA, USA, 15–17 June 1988; pp. 1691–1696.
21. Stein, G.; Doyle, J.C. Beyond singular values and loop shapes. *J. Guid. Control Dyn.* **1991**, *14*, 5–16. [CrossRef]
22. McFarlane, D.; Glover, K. A loop-shaping design procedure using H/sub infinity/synthesis. *IEEE Trans. Autom. Control* **1992**, *37*, 759–769. [CrossRef]
23. Rahman, M.Z.U.; Liaquat, R.; Rizwan, M.; Martin-Barreiro, C.; Leiva, V. A robust controller of a reactor electromicrobial system based on a structured fractional transformation for renewable energy. *Fractal Fract.* **2022**, *6*, 736. [CrossRef]
24. Khalil, I.S.; Doyle, J.C.; Glover, K. *Robust and Optimal Control*; Prentice Hall: New York, NY, USA, 1996.
25. Gahinet, P.; Apkarian, P. Decentralized and fixed-structure H∞ control in MATLAB. In Proceedings of the 50th IEEE Conference on Decision and Control and European Control Conference, Orlando, FL, USA, 12–15 December 2011; pp. 8205–8210.
26. Diab, A.A.Z.; Al-Sayed, A.H.M.; Abbas Mohammed, H.H.; Mohammed, Y.S. Robust speed controller design using H∞ theory for high performance sensorless induction motor drives. In *Development of Adaptive Speed Observers for Induction Machine System Stabilization*; Springer: Singapore, 2019.
27. Brezina, L.; Brezina, T. H-infinity controller design for a DC motor model with uncertain parameters. *Eng. Mech.* **2011**, *18*, 271–279.
28. Dey, N.; Mondal, U.; Mondal, D. Design of a H-infinity robust controller for a DC servo motor system. In Proceedings of the 2016 International Conference on Intelligent Control Power and Instrumentation, Kolkata, India, 21–23 October 2016; pp. 27–31.
29. Krishnan, T.D.; Krishnan, C.M.C.; Vittal, K.P. Design of robust H-infinity speed controller for high performance BLDC servo drive. In Proceedings of the 2017 International Conference on Smart grids, Power and Advanced Control Engineering, Bangalore, India, 17–19 August 2017; pp. 37–42.

30. Apkarian, P.; Bompart, V.; Noll, D. Non-smooth structured control design with application to PID loop-shaping of a process. *Int. J. Robust Nonlinear Control* **2007**, *17*, 1320–1342. [CrossRef]
31. Noll, D.; Apkarian, P.; Bompart, V. Nonsmooth structured control design. *IFAC Proc.* **2007**, *40*, 357–362. [CrossRef]
32. Kaitwanidvilai, S.; Parnichkun, M. Genetic-algorithm-based fixed-structure robust h loop-shaping control of a pneumatic servo system. *J. Robot. Mechatron.* **2004**, *16*, 362–373. [CrossRef]
33. Koch, G.G.; Osorio, C.R.; Pinheiro, H.; Oliveira, R.C.; Montagner, V.F. Design procedure combining linear matrix inequalities and genetic algorithm for robust control of grid-connected converters. *IEEE Trans. Ind. Appl.* **2019**, *56*, 1896–1906. [CrossRef]
34. Schirrer, A.; Westermayer, C.; Hemedi, M.; Kozek, M. Robust H∞ control design parameter optimization via genetic algorithm for lateral control of a BWB type aircraft. *IFAC Proc.* **2010**, *43*, 57–63. [CrossRef]
35. Ramirez-Figueroa, J.A.; Martin-Barreiro, C.; Nieto, A.B.; Leiva, V.; Galindo-Villardón, M.P. A new principal component analysis by particle swarm optimization with an environmental application for data science. *Stoch. Environ. Res. Risk Assess.* **2021**, *35*, 1969–1984. [CrossRef]
36. Singh, V.P.; Mohanty, S.R.; Kishor, N.; Ray, P.K. Robust H-infinity load frequency control in hybrid distributed generation system. *Int. J. Electr. Power Energy Syst.* **2013**, *46*, 294–305. [CrossRef]
37. Singh, V.P.; Kishor, N.; Samuel, P.; Mohanty, S.R. Impact of communication delay on frequency regulation in hybrid power system using optimized H-infinity controller. *IETE J. Res.* **2016**, *62*, 356–367. [CrossRef]
38. Zhao, J.; Gao, Z.M. The fully informed mayfly optimization algorithm. In Proceedings of the 2020 International Conference on Big Data and Artificial Intelligence and Software Engineering, Chengdu, China, 23–25 October 2020; pp. 450–453.
39. MatLab Team. *Robust Control Toolbox 4.1*; The Math Works, Inc.: Natick, MA, USA, 2011.
40. Rahman, M.Z.U.; Shaikh, I.U.H.; Ali, A.; Ahmad, N. Fixed-structure Hα control of couple tank system and anti-integral windup PID control strategy for actuator saturation. In Proceedings of the 2016 World Congress on Industrial Control Systems Security, London, UK, 12–14 December 2016; pp. 1–6.
41. Mehta, V.K.; Mehta, R. *Principles of Electrical Machines*; Chand Publishing: New Delhi, India, 2008.
42. Inteco. Manual. In *Modular Servo System (MSS). User's Manual*; Inteco: Krakow, Poland, 2006.
43. Borase, R.P.; Maghade, D.K.; Sondkar, S.Y.; Pawar, S.N. A review of PID control, tuning methods and applications. *Int. J. Dyn. Control* **2021**, *9*, 818–827. [CrossRef]
44. Shi, T.; Su, H.; Chu, J. Reliable H-infinity filtering for linear systems with sensor saturation. *J. Control Theory Appl.* **2013**, *11*, 80–85. [CrossRef]
45. Gahinet, P.; Apkarian, P. Structured H_∞ synthesis in MATLAB. *IFAC Proc.* **2011**, *44*, 1435–1440. [CrossRef]